Resonant evanescent excitation of OAM modes in a high-contrast circular step-index fiber

Hammer, Manfred, Ebers, Lena, Förstner, Jens

Manfred Hammer, Lena Ebers, Jens Förstner, "Resonant evanescent excitation of OAM modes in a high-contrast circular step-index fiber," Proc. SPIE 12017, Complex Light and Optical Forces XVI, 120170F (2 March 2022); doi: 10.1117/12.2612179

SPIE.

Event: SPIE OPTO, 2022, San Francisco, California, United States

Invited Paper

Resonant evanescent excitation of OAM modes in a high-contrast circular step-index fiber

Manfred Hammer, Lena Ebers, Jens Förstner

Paderborn University, Theoretical Electrical Engineering, Paderborn, Germany

ABSTRACT

Resonant evanescent coupling can be utilized to selectively excite orbital angular momentum (OAM) modes of high angular order supported by a thin circular dielectric rod. Our 2.5-D hybrid-analytical coupled mode model combines the vectorial fields associated with the fundamental TE- and TM-modes of a standard silicon photonics slab waveguide, propagating at oblique angles with respect to the rod axis, and the hybrid modes supported by the rod. One observes an efficient resonant interaction in cases where the common axial wavenumber of the waves in the slab matches the propagation constant of one or more modes of the rod. For certain modes of high angular order, the incident wave is able to transfer its directionality to the field in the fiber, exciting effectively only one of a pair of degenerate OAM modes.

Keywords: photonics, integrated optics, dielectric resonators, modes of dielectric step-index fibers, orbital angular momentum modes, OAM modes, resonant evanescent coupling, oblique excitation, semi-guided waves

1. INTRODUCTION

Optical microresonators can be counted among the standard building blocks of integrated photonic circuits.[1,2] Frequently, these are realized with a circular, ring- or disk-shaped cavity, that is evanescently coupled to one or more close-by bus waveguides. Traveling wave resonances are excited, which could be regarded as optical "vortex" fields,[3,4] of extreme angular order, and with excellent purity.[5] By construction, however, the waves remain localized in the cavity, and as such might not be of immediate interest in a context of research on OAM waves,[6–8] on electromagnetic waves that carry optical angular momentum.[9–12] The latter have been studied for quite some time, with potential applications ranging from interest in the mechanical torque[9] to optical telecommunications[12] and nonlinear and quantum optics.[11] Methods for the generation of OAM waves target either free-space vortex beams or specific OAM modes in circular optical fibers. The proposals include spiral phase plates,[13] tailored lens arrangements,[14] spatial light modulators,[15] and helical gratings,[16,17] as well as other grating- or metasurface-based devices, but also sophisticated proposals like steered fiber couplers,[18] or even nonlinear excitation schemes.[19]

Recently we have investigated an alternative configuration,[20,21] that combines, in a certain sense, concepts from the realms of circular optical microresonators and of OAM waves. We consider a thin dielectric high-contrast step index fiber, or a long circular dielectric rod, respectively, that is coupled to a slab waveguide at some distance underneath. Fig. 1 shows a schematic of the setup. The evanescent interaction between the fiber and the semi-guided waves supported by the slab can be analyzed conveniently in terms of a 2.5-D coupled mode model,[20] that gives direct access to the amplitudes of the individual OAM modes of the fiber. The model predicts a strong resonant interaction if the incoming waves and the relevant fiber mode meet certain phase matching conditions, i.e. if the exciting semi-guided plane wave in the slab comes in at a specific angles. Realistic 3-D solutions, with incoming semi-guided wave bundles of e.g. Gaussian shape, can be assembled by combining the former 2.5-D fields.[21,22] For our previous studies in Refs. 20, 21 we considered fibers in the form of dielectric rods with a thin, high-index coating, i.e. with the annular refractive index profiles of dielectric "tubes". In that case, the cylindrical outer layer of the tube supports a series of OAM modes that are well separated, in effective index, from the bunch of fiber modes found for the core rod.

To further this topic, in this paper we discuss the oblique excitation of the plain rod of Fig. 1 without the coating layer, where the interesting OAM modes of higher angular order are mixed with the multitude of other rod modes. Section 2 takes a look at the mode spectrum of the multimode high-contrast fiber. Next, in Sections 3, 4, we discuss the oblique

M. Hammer, Paderborn University, Theoretical Electrical Engineering, Warburger Straße 100, 33098 Paderborn, Germany, Phone: ++49 (0)5251/60-3560, Fax: ++49 (0)5251/60-3524, E-mail: manfred.hammer@uni-paderborn.de

Complex Light and Optical Forces XVI, edited by David L. Andrews, Enrique J. Galvez, Halina Rubinsztein-Dunlop, Proc. of SPIE Vol. 12017, 120170F
 · 0277-786X · doi: 10.1117/12.2612179

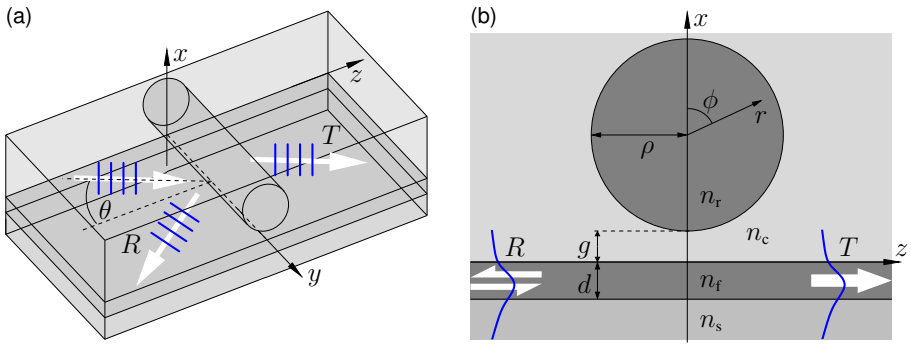

Figure 1. Oblique evanescent excitation of a circular dielectric rod, schematic (a), and cross section view (b). Cartesian coordinates x, y, z are oriented such that x is normal to the slab plane, with the y-axis parallel to the rod; polar coordinates r, ϕ are positioned at the rod axis. TE excitation at vacuum wavelength $\lambda = 1.55\,\mu$m; the incoming semi-guided wave propagates in the y-z-plane at an angle θ with respect to the z-axis. Outgoing TE polarized waves with reflectance R and transmittance T are observed under the same angle. Parameters: refractive indices $n_\mathrm{f} = n_\mathrm{r} = 3.45$ (rod and film core), $n_\mathrm{s} = 1.45$ (substrate), $n_\mathrm{c} = 1.0$ (cladding), slab thickness $d = 0.22\,\mu$m, variable rod radius ρ and gap g.

evanescent excitation of the rod by semi-guided plane waves, and comment briefly on the coupled mode model that forms the basis for the simulations in this paper. Section 6 highlights a series of resonances for OAM modes with increasing angular order. The last Section 7 shows some results for the excitation by semi-guided Gaussian wave bundles with limited lateral extension.

2. MODE SPECTRUM

The parameters introduced in Fig. 1 resemble typical values for standard high-contrast waveguides of silicon photonics.[23] To facilitate the selective excitation, the modes supported by the dielectric rod should preferably be distributed over a large effective index range. Hence we also assume the rod to be made of silicon, with air background, as considered for the former tubes in Ref. 21. Fig. 2 shows effective indices of the guided modes supported by the separate rod, as a function of the rod radius ρ.

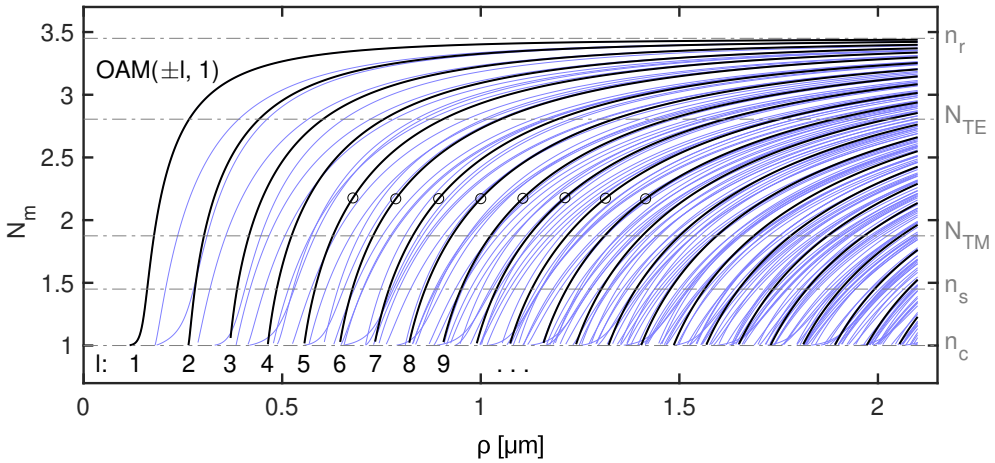

Figure 2. Effective indices N_m of the TE-, TM-, and OAM modes supported by the dielectric rod of Fig. 1, for absent slab waveguide, versus the rod radius ρ. Black solid lines correspond to the fundamental OAM$(\pm l, 1)$-modes of angular order l; the lighter blue curves show the effective indices of all other modes. The dash-dotted horizontal lines show the levels of the core, cladding, and substrate refractive indices n_r n_c, n_s, and the effective indices N_TE, N_TM of the slab modes. Markers indicate the configurations of Figs. 4 and 5.

The high-contrast rod represents a highly multimode waveguide, where the density of effective indices, on the range between n_c and n_r permitted for guided modes, increases with rod radius. Crossings of dispersion curves belonging to modes of different angular order are not forbidden, and can be observed in several places in Fig. 2.

The guided eigenmodes are considered here as separable hybrid vectorial optical fields with electric part $\boldsymbol{E}$ and magnetic part $\boldsymbol{H}$, with vectorial radial profile function $\boldsymbol{\psi}$, real propagation constant $\beta = kN_{\mathrm{m}}$, and effective mode index N_{m}, for vacuum wavenumber k:

$$(\boldsymbol{E}, \boldsymbol{H})(r, \phi, y) = \boldsymbol{\psi}(r) \exp(-\mathrm{i}l\phi - \mathrm{i}\beta y). \tag{1}$$

Following standard theory for optical fibers,[24,25] separate eigenvalue problems can be established for modes with differing integer angular orders l. Analytical solutions[26,27] are available for the present simulations. Modes OAM(l, m), for $l \geq 1$, are characterized by two indices. Next to l, a second index m counts modes with that angular order, sorted according to decreasing effective indices. Fields OAM$(\pm l, m)$ with opposite angular order are exactly degenerate; the familiar EH- and HE-modes of optical fibers can be assembled as superpositions of these degenerate fields. Further, for angular order 0, the series of transverse electric (TE) and transverse magnetic (TM) modes are labeled TE$(0, m)$ and TM$(0, m)$, respectively.

As an example, for the radius $\rho = 1\,\mu\mathrm{m}$, our solvers identify in total the 48 modes TE$(0, m)$ and TM$(0, m)$, $m = 1, \ldots, 4$, further modes OAM$(1, 1)$ – OAM$(1, 8)$, OAM$(2, 1)$ – OAM$(2, 7)$, OAM$(3, 1)$ – OAM$(3, 6)$, OAM$(4, 1)$ – OAM$(4, 5)$, OAM$(5, 1)$ – OAM$(5, 4)$, OAM$(6, 1)$ – OAM$(6, 3)$, OAM$(7, 1)$ – OAM$(7, 2)$, OAM$(8, 1)$ – OAM$(8, 2)$, OAM$(9, 1)$ – OAM$(9, 2)$, and OAM$(10, 1)$. Among these, modes with higher second index show larger field levels rather in the interior of the rod, while the fields of modes with low second index $m = 1, 2$ tend to be concentrated near the outer rim. One thus can expect the latter to be more amenable to external evanescent excitation.

3. OBLIQUE EVANESCENT EXCITATION

The composite rod-waveguide-structure of Fig. 1 is constant along the rod axis y. In place of a traditional 2-D treatment, with solutions that are also constant along y, i.e. fields that correspond to perpendicular incidence, here we need to consider oblique incidence of the modes guided in the slab, where the fields are varying harmonically along y. "2.5-D"-configurations like this show certain peculiarities,[28] which have been exploited for a series of device proposals in the recent past. Among these are simple mirrors, power splitters, and slab waveguide transitions,[29–32] step- and corner-folds in slab waveguides,[22,33,34] and configurations that realize a variety of filter functions through the oblique excitation of channel waveguides with rectangular cross sections.[35–45] Also Refs. 20, 21 belong to this list. Following the detailed reasoning[28] in those papers, a few immediate conclusions can be drawn for the present structure.

The slab waveguide with parameters as given in the caption of Fig. 1 supports fundamental guided TE and TM modes with effective indices $N_{\mathrm{TE}} = 2.8051$, $N_{\mathrm{TM}} = 1.8748$, respectively.[46] With its higher effective index, the TE mode enables resonant interaction with a far larger range of OAM modes (cf. Section 5) than the TM mode. Hence, for reasons of brevity, we will discuss TE excitation only. An incoming semi-guided plane wave propagating at angle θ is characterized by a wavenumber $k_y = kN_{\mathrm{TE}} \sin\theta$ in y-direction. One can then restrict the total optical electromagnetic field to that particular component of a Fourier decomposition along y, i.e. all optical fields are assumed to vary along y with that common wavenumber.

Consequently, some propagating outgoing wave with effective index N_{out} is observed at an angle θ_{out} which is related to the angle of incidence by a variant of Snell's law:

$$k_y = kN_{\mathrm{TE}} \sin\theta = kN_{\mathrm{out}} \sin\theta_{\mathrm{out}}, \quad \text{or} \quad N_{\mathrm{TE}} \sin\theta = N_{\mathrm{out}} \sin\theta_{\mathrm{out}}. \tag{2}$$

This requires that N_{out} is sufficiently high. Otherwise, that wave becomes evanescent what concerns the propagation in the cross sectional x-z-plane, i.e. it does not transport optical power. Hence, for each particular outgoing wave, a critical angle θ_{cr} can be defined as $\sin\theta_{\mathrm{cr}} = N_{\mathrm{out}}/N_{\mathrm{TE}}$, such that the wave is evanescent for incidence at angles $\theta > \theta_{\mathrm{cr}}$.

Specifically for the present structure, using the relations $\sin\theta_{\mathrm{c,\,s}} = n_{\mathrm{c,\,s}}/N_{\mathrm{TE}}$ one calculates critical angles $\theta_{\mathrm{c}} = 20.88°$ and $\theta_{\mathrm{s}} = 31.13°$ for radiative losses to any nonguided fields in the cladding (c) and substrate regions (s). Thus, for wave incidence above θ_{s}, the structure becomes essentially lossless. What concerns the excitation of TM modes, a critical angle of $\theta_{\mathrm{TM}} = 41.94°$ applies, with $\sin\theta_{\mathrm{TM}} = N_{\mathrm{TM}}/N_{\mathrm{TE}}$. For TE excitation at larger angles, outgoing TM modes are suppressed. Then the entire input power is carried away from the central region of interaction by the reflected and transmitted TE modes.

4. HYBRID COUPLED MODE MODEL

All results for the slab-rod structure shown in this paper have been calculated by a specific, hybrid-analytical / numerical variant (HCMT)[47] of coupled mode theory.[48–50] Starting point is a physically plausible ansatz, an approximate "template", for the optical electromagnetic field. Vectorial expressions for the fundamental directional TE- and TM-modes of the slab are superimposed with amplitudes that are functions of their propagation coordinate z. On a suitable computational interval these amplitude functions are discretized in terms of standard 1-D linear finite-elements. A selection of the vectorial OAM or TE/TM modes represents the field in the rod. These are superimposed with a-priori unknown amplitudes. Then a projection procedure of Galerkin-type, for the source-free Maxwell equations in the frequency-domain, allows to establish a linear system of equations for all unknown coefficients, which is solved numerically. We refer to Refs. 20, 51 for details of the technique.

The simulations in this paper rely on a template, where the amplitudes of the directional polarized slab modes are discretized on an interval $z \in [-4, 4]$ µm with a regular stepsize 0.05 µm. Fiber modes with characteristic angles θ_m (cf. the next section) in an interval $[\theta - 10°, \theta + 10°]$ around the angle of incidence θ are included. Reflectances R_TE, R_TM and transmittances T_TE, T_TM for the fundamental TE and TM slab modes add up to unity, within the limits of numerical accuracy. Excellent agreement between the approximate HCMT model and rigorous numerical finite-element computations[52] has been observed[20] so far; for the present paper we confirmed the results for the resonant configurations of Section 6.

5. ANGULAR SPECTRUM OF THE EVANESCENTLY EXCITED ROD

For a particular rod mode with effective index N_m, one can expect a resonant interaction, if the wavenumber $k_y = kN_\mathrm{TE} \sin\theta$ of the incoming semi-guided wave in the slab comes close to the propagation constant kN_m of that mode. A characteristic angle θ_m can be associated with each rod mode, defined by the relation $\sin\theta_\mathrm{m} = N_\mathrm{m}/N_\mathrm{TE}$. Note that, even for excitation at the appropriate angle $\theta \approx \theta_\mathrm{m}$, there are further conditions that determine the actual strength of the resonance features.

With angles of incidence θ between θ_s, the critical angle for radiative losses, and grazing incidence near $90°$, only a range of OAM modes with effective indices between n_s and N_TE can be accessed. These levels are indicated in Fig. 2. Fig. 3 shows a respective spectrum for a moderate sized rod of radius $\rho = 1$ µm, for a not too narrow gap $g = 300$ nm.

Fig. 2 shows manifold regions, where dispersion curves come close to each other. For those parameters, resonances must be expected where multiple neighboring OAM modes contribute with nonnegligible amplitudes. This is indeed the case for stronger interaction at narrower gaps (not shown here; cf. the series of spectra in Refs. 20). For the 300 nm gap of Fig. 3, however, the features observed in the reflectance and transmittance curves can mostly be associated with merely one or a degenerate pair of the rod modes, that exhibit large amplitudes at the respective angular positions. Note that polarization conversion is suppressed for $\theta > \theta_\mathrm{TM}$; the curves R_TM and T_TM are zero in that angular range.

Resonances of the OAM modes with indices $m > 2$ ("other"), and of the TE and TM modes of the rod, respectively, show up mostly by a sharp dip in transmittance, and a corresponding reflectance peak. This points at a resonance of "standing wave" -type[53] as observed for the rectangular microstrip in Ref. 38, with an extremal state of large/full reflectance. In case of the OAM modes, both of the degenerate modes with positive and negative angular order are excited with, on the scale of the figure, large amplitudes of comparable magnitude. Hence, just as for the TE and TM modes of zero angular order, the (still strong) resonant field in the rod does not / hardly show any net orbital angular momentum.

This is different for the OAM modes of lower mode index $m = 1, 2$, at least for those with not too large mode angles. Their resonances do hardly (or not at all) show up in the reflectance and transmittance curves (exception: OAM$(9, 1)$, a small peak/dip in the T_TE- and T_TM-curves hints at some polarization conversion). Of the two degenerate fields, only the modes OAM$(-l, m)$ of negative angular order are excited with substantial amplitudes, while the amplitudes of the OAM$(+l, m)$ variants are much lower, or are not discernible at all in the figure. One could thus classify these as resonances that are more of a "traveling-wave" type, analogously to the terminology in the field of integrated optical microresonators,[53] with extremal states of large/full transmittance. The effect is less pronounced for the modes OAM$(4, 2)$, OAM$(6, 1)$, OAM$(5, 2)$ with higher characteristic angles, i.e. for excitation closer to grazing incidence.

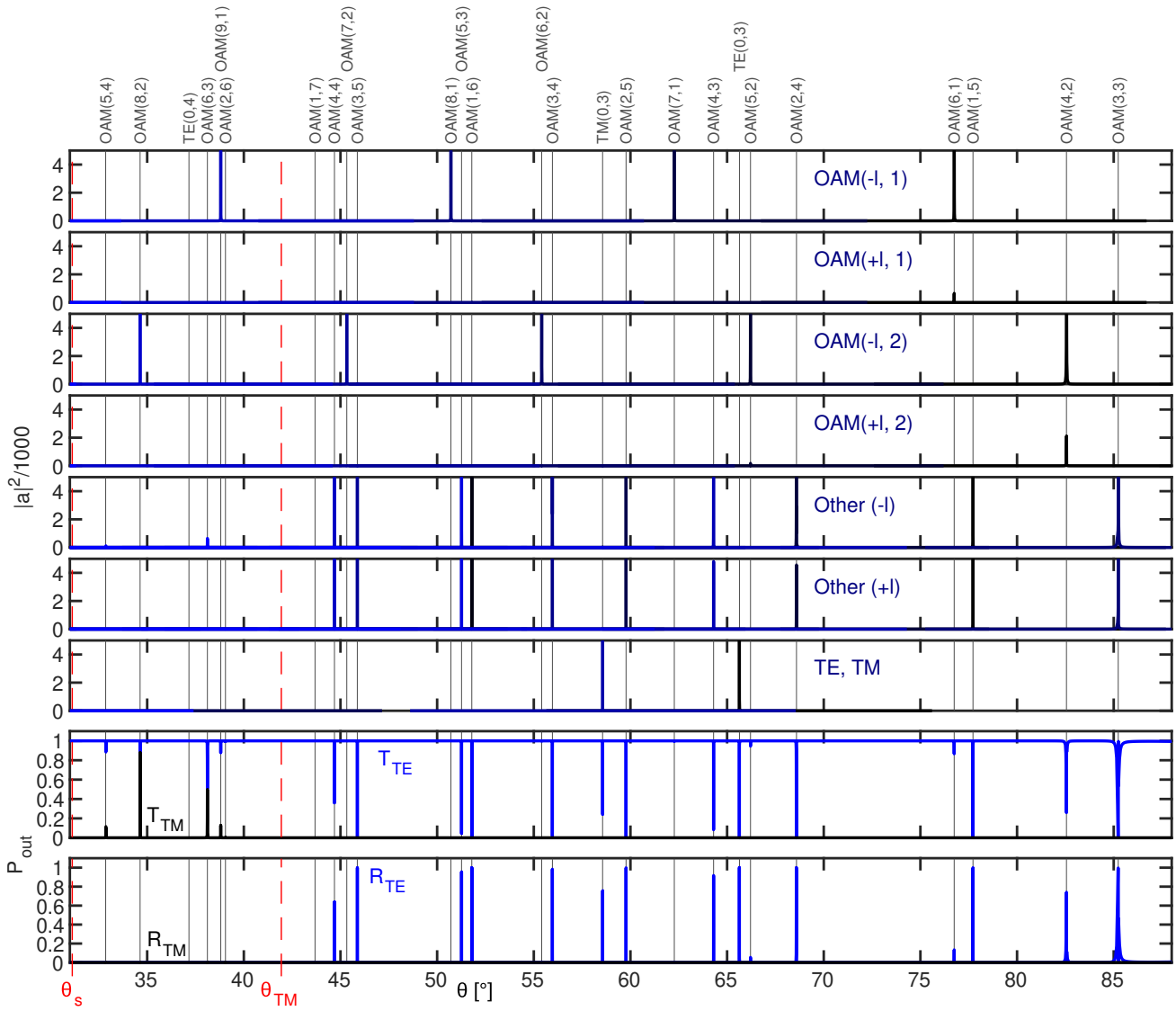

Figure 3. Oblique evanescent excitation of a dielectric rod of radius $\rho = 1$ µm, by TE-polarized semi-guided waves at angle of incidence θ, for a distance $g = 0.3$ µm between slab and rod. Panels, bottom to top: transmittances T_{TE}, T_{TM} and reflectances R_{TE}, R_{TM} for TE- and TM-polarized outgoing waves, and amplitudes $|a|^2$ of selected rod modes. Groups of modes with the same index 1, 2, "other" and the same sign of the angular mode order l share the same axes; respective peaks can be identified by close-by thin solid vertical lines at the positions of the respective mode angles θ_{m}. Dashed vertical lines indicate the critical angles θ_{s} and θ_{TM} for radiative losses / for scattering to TM polarized waves, respectively.

6. ROD RESONANCES

Primary interest in this paper is in the excitation of guided optical waves with high vorticity. We thus specialize to the OAM$(\pm l, 1)$-modes, indicated by the bold curves in Fig. 2. More specifically, we look at a region of effective indices in the middle of the accessible regime between n_s and N_TE with still moderate angles of incidence, but where also polarization conversion does not complicate matters (above N_TM). Rather arbitrarily we pick a level of roughly 2.17, given by the effective index of the OAM$(\pm 8, 1)$-mode for $\rho = 1.0\,\mu\mathrm{m}$ (these are the parameters of Fig. 3). By imagining a line at that level in Fig. 2, one can identify a series of radii (markers), where the rod supports OAM$(\pm l, 1)$-modes with effective indices close to that level. In what follows, we take a closer look at that series of configurations.

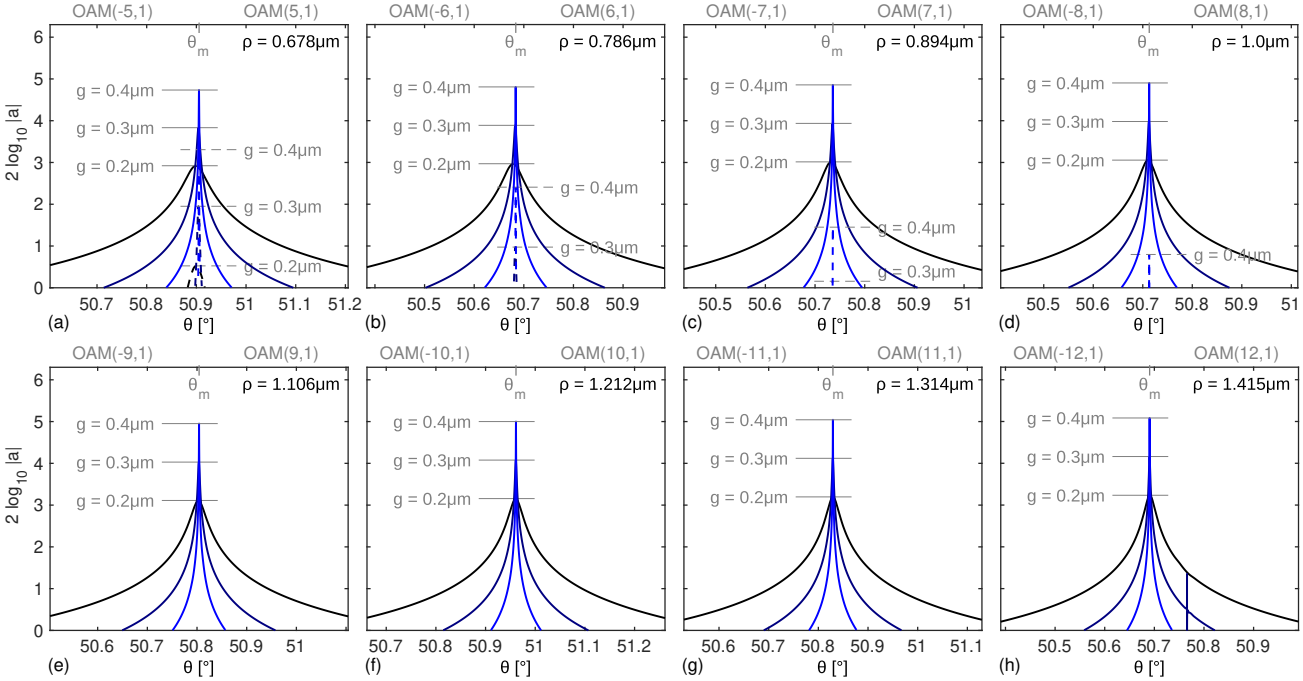

Figure 4. Amplitudes a of selected rod modes, excited by semi-guided TE waves at angle θ, for configurations with rod radius ρ and distances g between slab and rod. Each panel focuses on one doubly degenerate rod mode; curves can be assigned to the mode labels at the top of the panels by the maximum levels (horizontal lines) for specific gaps. Continuous lines correspond to the mode with negative angular order, dashed lines relate to the mode with positive angular order, if present. An additional upper tick mark indicates the characteristic angle θ_m for the mode pair.

Fig. 4 collects detailed angular scans of the resonances, now for different distances g between rod and slab. Each panel shows, on a logarithmic scale, the amplitudes assigned to a pair of degenerate modes OAM$(-l, 1)$ and OAM$(+l, 1)$ that constitute the resonance. What concerns the peak positions, as to be expected, for growing gap the resonances converge towards the mode angle θ_m for that pair of OAM modes; the coupling induced phase shift decreases.

Concerning extremal amplitude levels and resonance widths, we recover features as have been observed for the slab-coupled microstrip of Ref. 38. Accepting the model approximations of vanishing material losses and ideal surfaces, these structures can be regarded as resonator configurations with lossless cavities. Respective analytical models[25,54] predict an unlimited growth of resonance amplitudes, a decrease of resonance widths, and consequently a growth of the quality factor, for decreasing interaction strength, here for growing gap. Specifically, the roughly equally spaced maximum levels for the 100 nm steps in g hint at an exponential growth with gap distance of the maximum mode amplitudes.

At the same time one sees a strong inequality of the amplitude levels attained by OAM modes with negative and positive angular order. The inequality becomes even more pronounced for the configurations that concern modes with larger absolute angular order $|l|$ (in panels (e) to (h) of Fig. 4, the amplitudes $|a|^2$ for modes OAM$(+l, 1)$ are below 1, i.e. outside the range of the graphs). In those cases the rod is excited with a strong vortex field, consisting almost exclusively of the one OAM mode with negative angular order. Apparently, the incoming wave is able to transfer its directionality to the resonant field in the rod. These findings agree largely with observations for the tube-shaped fibers in Refs. 20, 21.

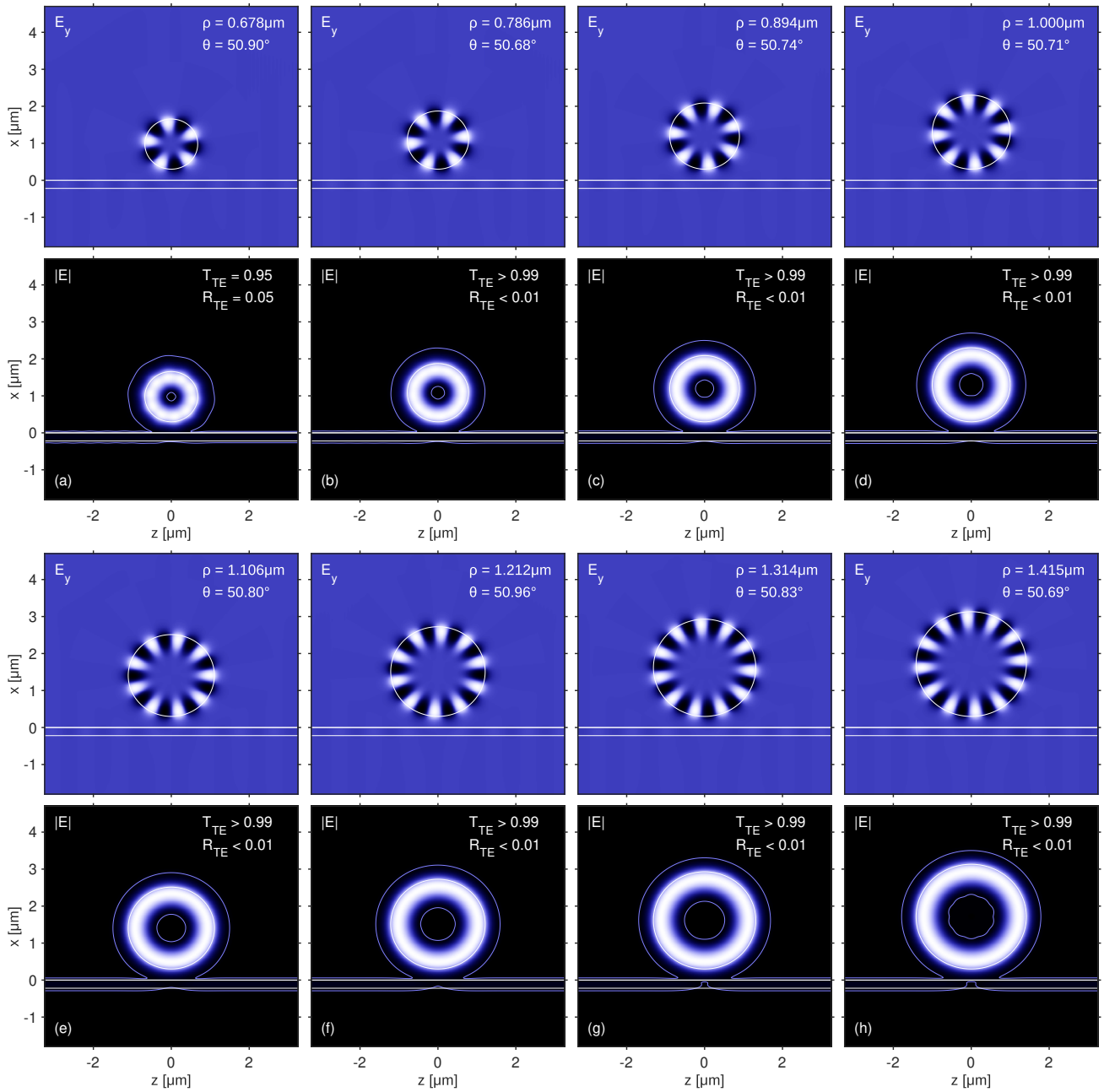

Figure 5. Cross-sectional fields E_y (axial electric field component, snapshots of the real physical field) and $|\boldsymbol{E}|$ (modulus of the vectorial electric field) for excitation of rods of radii ρ by TE-polarized waves at angles θ that correspond to the maximum levels in Fig. 4, for gaps $g = 0.3\,\mu\text{m}$. Color scales are adapted to the separate panels, with a contour at 1% of the field maxima ($|\boldsymbol{E}|$ only). The global phase for the E_y-plots has been chosen such that the field maxima become visible. Levels of transmittance T_{TE} and reflectance R_{TE} for TE-polarized semi-guided waves are shown.

Fig. 5 illustrates the corresponding resonant field patterns, for the configurations of Fig. 4, and for excitation at the resonance angles for gap $g = 300\,\mathrm{nm}$. The time snapshots of the physical axial electric fields show the angular periodicity that corresponds to the orders 5 – 12 of the OAM modes which constitute the resonances in parts (a) – (h) of the figure. Merely for the OAM mode of lowest order 5 (a), the plot of the absolute electric field shows a slight modulation, which indicates a contribution of the mode with opposite angular order. Otherwise, these are rather "pure" OAM fields with definite orbital angular momentum.

More quantitatively, for the present superpositions of power normalized rode modes, one can consider "purity" levels $p_i = |a_i|^2 / \sum_j |a_j|^2$ for each mode with index i in turn, where the sum runs over all rod modes that make up the composite fields, i.e. runs over all modes included in the HCMT template. We observe deviations $1 - p$ from pure fields of $1 \cdot 10^{-2}$ (OAM$(-5, 1)$, (a)), $1 \cdot 10^{-3}$ (OAM$(-6, 1)$, (b)), $2 \cdot 10^{-4}$ (OAM$(-7, 1)$, (c)), $3 \cdot 10^{-5}$ (OAM$(-8, 1)$, (d)), $2 \cdot 10^{-6}$ (OAM$(-9, 1)$, (e)), $2 \cdot 10^{-6}$ (OAM$(-10, 1)$, (f)), $5 \cdot 10^{-6}$ (OAM$(-11, 1)$, (g)), and $4 \cdot 10^{-5}$ (OAM$(-12, 1)$, (h)). Note, however, that these numbers originate from an inherently approximate model and from calculations with limited numerical accuracy.

7. EXCITATION BY SEMI-GUIDED GAUSSIAN BEAMS

Finally, we consider briefly the excitation of the rod by Gaussian bundles of semi-guided waves, i.e. by fields of limited extension along y. True 3-D solutions for these scenarios are realized as Fourier series that superimpose the former 2.5-D results for a range of wavenumbers k_y, or for a range of angles of incidence, respectively. We refer to Refs. 21, 22 for detailed expressions. The incoming semi-guided beam is spatially and spectrally of Gaussian shape and characterized by a width W (the full width of the field at level $1/\mathrm{e}$, measured at the beam focus in the direction perpendicular to the beam axis), and by a principal angle of incidence θ_0. As an example, Fig. 6 shows the illumination of the rod of Figs. 4(e) and 5(e) by a beam of 5 mm width, oriented at the resonance angle for the 300 nm gap, focused at the coordinate origin.

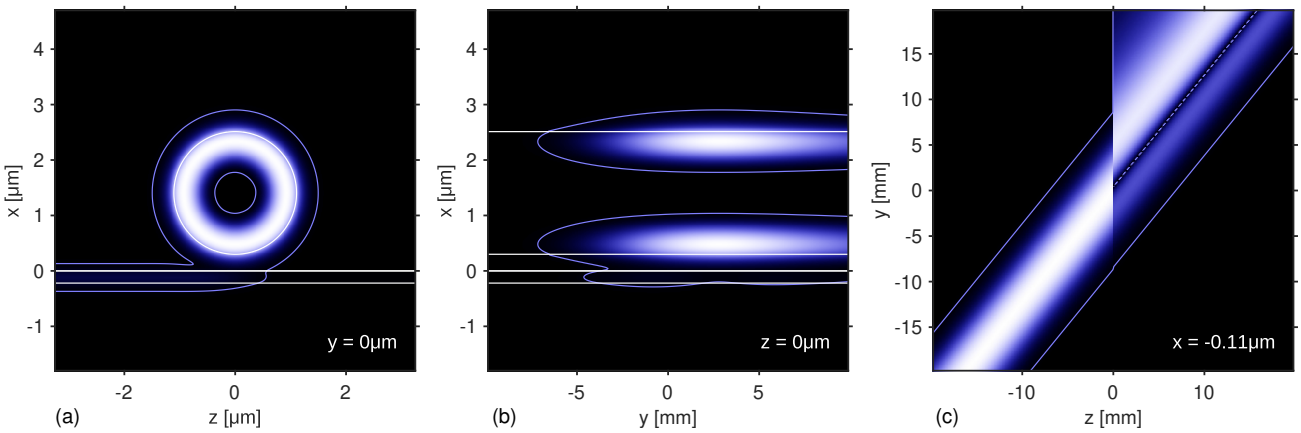

Figure 6. Excitation of a dielectric rod of radius $\rho = 1.106\,\mu\mathrm{m}$ by a TE-polarized semi-guided Gaussian wave bundle of cross-sectional width $W = 5\,\mathrm{mm}$ at angle $\theta_0 = 50.8037°$, for gap $g = 0.3\,\mu\mathrm{m}$. The panels show the absolute electric field $|\boldsymbol{E}|$ on the fiber cross section plane at $y = 0\,\mu\mathrm{m}$ (a), on the vertical plane including the fiber axis at $z = 0\,\mu\mathrm{m}$ (b), and on the horizontal plane at the slab center $x = -d/2$ (c). Color scales are adapted to the field range on the individual plots, with a contour at 1% of the respective maxima.

But for the mostly absent ongoing wave in the slab region, the field on the fiber cross section at the origin (a) appears very similar to Fig. 5(e). According to panels (b) and (c), a substantial part of the incoming optical power enters the rod, and then leaks back into the slab while propagating along the fiber. Panel (b) shows a maximum intensity in the rod at positions y a little beyond 2 mm. Beyond the uniform y-dependence, all parts of the optical field appear to propagate exclusively in positive z-, or negative ϕ-direction, respectively. Reflections, which would be visible as a modulation of the field in the slab in (a), or as a minor beam traveling in $-z/+y$-direction in (c), are entirely absent.

Following largely the recipes detailed in Ref. 21, the width W of the incoming beam has been roughly optimized for maximum power transfer. Our model predicts that 80.2% of the input power is channeled to the OAM$(-9, 1)$ mode at the intensity maximum at $y = 2.8\,\mathrm{mm}$. The purity levels as given in Section 6 apply. The ratio between the field maxima (squared electric field $|\boldsymbol{E}|^2$) in the rod at this position and the maximum level in the input beam is estimated at about 400. Thus, if the setup is intended as a source for high-order OAM waves, the slab should end at the x-z-plane at this y-position.

8. CONCLUSION

Vortex waves of high angular order and of excellent purity can be generated by resonant evanescent coupling between a thin circular dielectric rod and a close-by slab waveguide. Subject to certain resonance conditions, the incoming semi-guided wave excites effectively only one of a pair of degenerate orbital-angular-momentum modes in the rod. We confirmed the possibility of selective coupling, even for the dense eigenmode spectrum of the present highly multimode fibers. Further, semi-guided beams of limited width can couple a major part of their input power to the vortex fields. For our example we estimate a maximum power transfer of 80%, accompanied by an enhancement of squared electric fields by a factor of about 400. The results confirm that previous observations on configurations with tube shaped fibers, with annular refractive index profiles, largely apply to the simpler dielectric rods of the present paper.

ACKNOWLEDGMENTS

Financial support from the German Research Foundation (Deutsche Forschungsgemeinschaft DFG, project 231447078–TRR 142, subproject C05) is gratefully acknowledged.

REFERENCES

[1] Michelotti, F., Driessen, A., and Bertolotti, M., eds., [*Microresonators as building blocks for VLSI photonics*], vol. 709 of AIP conference proceedings, American Institute of Physics, Melville, New York (2004).

[2] Schwelb, O. and Chremmos, I., "Band-limited microresonator reflectors and mirror structures," in [*Photonic Microresonator Research and Applications*], Chremmos, I., Uzunoglu, N., and Schwelb, O., eds., *Springer Series in Optical Sciences, Vol. 156*, 139–163, Springer, London (2010).

[3] Berry, M. V., "Optical currents," *Journal of Optics A: Pure and Applied Optics* **11**, 094001 (2009).

[4] Wang, J., "Advances in communications using optical vortices," *Photonics Research* **4**(5), B14–B28 (2016).

[5] Sun, C., Zhang, J., Xiong, B., Wang, J., Hao, Z., Wang, L., Han, Y., Li, H., and Luo, Y., "Analysis of OAM mode purity of integrated optical vortex beam emitters," *IEEE Photonics Journal* **9**(1), 1–7 (2017).

[6] Bozinovic, N., Yue, Y., Ren, Y., Tur, M., Kristensen, P., Huang, H., Willner, A. E., and Ramachandran, S., "Terabit-scale orbital angular momentum mode division multiplexing in fibers," *Science* **340**(6140), 1545–1548 (2013).

[7] Wang, L., Vaity, P., Chatigny, S., Messaddeq, Y., Rusch, L. A., and LaRochelle, S., "Orbital-angular-momentum polarization mode dispersion in optical fibers," *Journal of Lightwave Technology* **34**(8), 1661–1671 (2016).

[8] Johnson, J. D., Ma, Z., Padgett, M. J., and Ramachandran, S., "Measurement of the spin-orbit coupling interaction in ring-core optical fibers," *OSA Continuum* **2**(10), 2975–2982 (2019).

[9] Allen, L., Beijersbergen, M. W., Spreeuw, R. J. C., and Woerdman, J. P., "Orbital angular momentum of light and the transformation of laguerre-gaussian laser modes," *Physical Review A* **45**, 8185–8189 (1992).

[10] Franke-Arnold, S., Allen, L., and Padgett, M., "Advances in optical angular momentum," *Laser & Photonics Reviews* **2**(4), 299–313 (2008).

[11] Yao, A. M. and Padgett, M. J., "Orbital angular momentum: origins, behavior and applications," *Advances in Optics and Photonics* **3**(2), 161–204 (2011).

[12] Willner, A. E., Huang, H., Yan, Y., Ren, Y., Ahmed, N., Xie, G., Bao, C., Li, L., Cao, Y., Zhao, Z., Wang, J., Lavery, M. P. J., Tur, M., Ramachandran, S., Molisch, A. F., Ashrafi, N., and Ashrafi, S., "Optical communications using orbital angular momentum beams," *Advances in Optics and Photonics* **7**(1), 66–106 (2015).

[13] Oemrawsingh, S. S. R., van Houwelingen, J. A., Eliel, E. R., Woerdman, J. W., Verstegen, E. J. K., Kloosterboer, J. G., and 't Hooft, G. W., "Production and characterization of spiral phase plates for optical wavelengths," *Applied Optics* **43**(3), 688–694 (2004).

[14] Beijersbergen, M. W., Allen, L., van der Veen, H. E. L. O., and Woerdman, J. P., "Astigmatic laser mode converters and transfer of orbital angular momentum," *Optics Communications* **96**(1), 123–132 (1993).

[15] Zhu, L. and Wang, J., "Arbitrary manipulation of spatial amplitude and phase using phase-only spatial light modulators," *Scientific Reports* **4**, 7441 (2015).

[16] Lin, Z., Wang, A., Xu, L., Zhang, X., Sun, B., Gu, C., and Ming, H., "Generation of optical vortices using a helical fiber Bragg grating," *Journal of Lightwave Technology* **32**(11), 2152–2156 (2014).

[17] Fang, L. and Wang, J., "Mode conversion and orbital angular momentum transfer among multiple modes by helical gratings," *IEEE Journal of Quantum Electronics* **52**(8), 1–6 (2016).

[18] Yan, Y., Wang, J., Zhang, L., Yang, J.-Y., Fazal, I.-M., Ahmed, N., Shamee, B., Willner, A.-E., Birnbaum, K., and Dolinar, S., "Fiber coupler for generating orbital angular momentum modes," *Optics Letters* **36**(21), 4269–4271 (2011).
[19] Fan, J., Zhao, J., Shi, L., Xiao, N., and Hu, M., "Two-channel, dual-beam-mode, wavelength-tunable femtosecond optical parametric oscillator," *Advanced Photonics* **2**(4), 1–5 (2020).
[20] Hammer, M., Ebers, L., and Förstner, J., "Hybrid coupled mode modelling of the evanescent excitation of a dielectric tube by semi-guided waves at oblique angles," *Optical and Quantum Electronics* **52**, 472 (2020).
[21] Hammer, M., Ebers, L., and Förstner, J., "Resonant evanescent excitation of guided waves with high-order optical angular momentum," *Journal of the Optical Society of America B* **38**(5), 1717–1728 (2021).
[22] Hammer, M., Hildebrandt, A., and Förstner, J., "Full resonant transmission of semi-guided planar waves through slab waveguide steps at oblique incidence," *Journal of Lightwave Technology* **34**(3), 997–1005 (2016).
[23] Soref, R., "The past, present, and future of silicon photonics," *IEEE Journal of Selected Topics in Quantum Electronics* **12**(6), 1678–1687 (2006).
[24] Snyder, A. W. and Love, J. D., [*Optical Waveguide Theory*], Chapman and Hall, London, New York (1983).
[25] Okamoto, K., [*Fundamentals of Optical Waveguides*], Academic Press, SanDiego (2000).
[26] Hammer, M., "METRIC — Mode expansion tools for 2D rectangular integrated optical circuits." https://metric.computational-photonics.eu/.
[27] Hammer, M., "FiMS — Modes of circular multi-step index optical fibers." https://www.computational-photonics.eu/fims.html.
[28] Hammer, M., Ebers, L., Hildebrandt, A., Alhaddad, S., and Förstner, J., "Oblique semi-guided waves: 2-D integrated photonics with negative effective permittivity," in [*2018 IEEE 17th International Conference on Mathematical Methods in Electromagnetic Theory (MMET)*], 9–15 (2018).
[29] Çivitci, F., Hammer, M., and Hoekstra, H. J. W. M., "Semi-guided plane wave reflection by thin-film transitions for angled incidence," *Optical and Quantum Electronics* **46**(3), 477–490 (2014).
[30] Tresna, W. P., Putra, A. W. S., and Maruyama, T., "Optical-loss measurement of a silicon-slab waveguide," *Current Optics and Photonics* **4**(6), 551–557 (2020).
[31] Hammer, M., Ebers, L., and Förstner, J., "Configurable lossless broadband beam splitters for semi-guided waves in integrated silicon photonics," *OSA Continuum* **4**(12), 3081–3095 (2021).
[32] Hammer, M., Ebers, L., and Förstner, J., "Oblique quasi-lossless excitation of a thin silicon slab waveguide: a guided-wave variant of an anti-reflection coating," *Journal of the Optical Society of America B* **36**(9), 2395–2401 (2019).
[33] Hammer, M., Hildebrandt, A., and Förstner, J., "How planar optical waves can be made to climb dielectric steps," *Optics Letters* **40**(16), 3711–3714 (2015).
[34] Ebers, L., Hammer, M., and Förstner, J., "Oblique incidence of semi-guided planar waves on slab waveguide steps: Effects of rounded edges," *Optics Express* **26**(14), 18621–18632 (2018).
[35] Bezus, E. A., Bykov, D. A., and Doskolovich, L. L., "Bound states in the continuum and high-Q resonances supported by a dielectric ridge on a slab waveguide," *Photonics Research* **6**(11), 1084–1093 (2018).
[36] Doskolovich, L. L., Bezus, E. A., and Bykov, D. A., "Two-groove narrowband transmission filter integrated into a slab waveguide," *Photonics Research* **6**(1), 61–65 (2018).
[37] Bezus, E. A., Doskolovich, L. L., Bykov, D. A., and Soifer, V. A., "Spatial integration and differentiation of optical beams in a slab waveguide by a dielectric ridge supporting high-Q resonances," *Optics Express* **26**(19), 25156–25165 (2018).
[38] Hammer, M., Ebers, L., and Förstner, J., "Oblique evanescent excitation of a dielectric strip: A model resonator with an open optical cavity of unlimited Q," *Optics Express* **27**(7), 9313–9320 (2019).
[39] Chen, J. and Chu, P., "Phase-induced Fano antiresonance in a planar waveguide with two dielectric ridges," *Journal of the Optical Society of America B* **36**(12), 3417–3427 (2019).
[40] Nguyen, T. G., Ren, G., Schoenhardt, S., Knoerzer, M., Boes, A., and Mitchell, A., "Ridge resonance in silicon photonics harnessing bound states in the continuum," *Laser & Photonics Reviews* **13**(10), 1900035 (2019).
[41] Nguyen, T. G., Yego, K., Ren, G., Boes, A., and Mitchell, A., "Microwave engineering filter synthesis technique for coupled ridge resonator filters," *Optics Express* **27**(23), 34370–34381 (2019).
[42] Doskolovich, L. L., Bezus, E. A., and Bykov, D. A., "Integrated flat-top reflection filters operating near bound states in the continuum," *Photonics Research* **7**(11), 1314–1322 (2019).

[43] Bykov, D. A., Bezus, E. A., and Doskolovich, L. L., "Bound states in the continuum and strong phase resonances in integrated gires-tournois interferometer," *Nanophotonics* **9**(1), 83–92 (2020).

[44] Bezus, E. A., Bykov, D. A., and Doskolovich, L. L., "Integrated gires–tournois interferometers based on evanescently coupled ridge resonators," *Optics Letters* **45**(18), 5065–5068 (2020).

[45] Schoenhardt, S., Boes, A., Nguyen, T. G., and Mitchell, A., "Ridge resonators: impact of excitation beam and resonator losses," *Optics Express* **29**(17), 27092–27103 (2021).

[46] Hammer, M., "OMS — 1-D mode solver for dielectric multilayer slab waveguides." https://www.computational-photonics.eu/oms.html.

[47] Hammer, M., "Guided wave interaction in photonic integrated circuits — a hybrid analytical / numerical approach to coupled mode theory," in [*Recent Trends in Computational Photonics*], Agrawal, A., Benson, T., DeLaRue, R., and Wurtz, G., eds., *Springer Series in Optical Sciences* **204**, ch. 3, 77–105, Springer, Cham (2017).

[48] Vassallo, C., [*Optical Waveguide Concepts*], Elsevier, Amsterdam (1991).

[49] Hall, D. G. and Thompson, B. J., eds., [*Selected Papers on Coupled-Mode Theory in Guided-Wave Optics*], vol. MS 84 of *SPIE Milestone Series*, SPIE Optical Engineering Press, Bellingham, Washington USA (1993).

[50] Huang, W. P., "Coupled mode theory for optical waveguides: an overview," *Journal of the Optical Society of America A* **11**(3), 963–983 (1994).

[51] Hammer, M., "Hybrid analytical / numerical coupled-mode modeling of guided wave devices," *Journal of Lightwave Technology* **25**(9), 2287–2298 (2007).

[52] Comsol Multiphysics GmbH, Göttingen, Germany; http://www.comsol.com.

[53] Manolatou, C., Khan, M. J., Fan, S., Villeneuve, P. R., Haus, H. A., and Joannopoulos, J. D., "Coupling of modes analysis of resonant channel add-drop filters," *IEEE Journal of Quantum Electronics* **35**(9), 1322–1331 (1999).

[54] Hiremath, K. R. and Hammer, M., "Circular integrated optical microresonators: Analytical methods and computational aspects," in [*Photonic Microresonator Research and Applications*], Chremmos, I., Schwelb, O., and Uzunoglu, N., eds., *Springer Series in Optical Sciences, Vol. 156*, 29–59, Springer, London (2010).